Nonlinear Schrödinger solitons scattering off an interface

Helge Frauenkron

HLRZ c/o Forschungszentrum Jülich GmbH
D–52425 Jülich, Germany

e-mail: H.Frauenkron@fz-juelich.de

Abstract

We integrate the one-dimensional nonlinear Schrödinger equation numerically for solitons moving in external potentials. In particular, we study the scattering off an interface separating two regions of constant potential modeled by a linear ramp. Transmission coefficients and inelasticities are computed as functions of the potential difference and the slope of the ramp. Our data show that the ramp's slope has a strong influence revealing unexpected windows of reflection in a transmission regime. The transmission coefficients for very small potential differences are compared with the theoretical predictions derived by perturbation theory. Also the time evolution of the solitary waves after the scattering is studied. We observed that they in general behave like solitons with an amplified amplitude. Due to this, they oscillate. The oscillation period is measured and compared with theoretical predictions.

PACS number(s): 03.40.Kf, 0.3.65.Ge, 42.65.Tg, 42.81.Dp

Key words: Nonlinear Schrödinger equation, Solitons, External potential, Transmission coefficients, Amplified solitons, Amlitude oscillation

1 Introduction

Recent years have seen a considerable growth in the interest for nonlinear partial differential equations with soliton solutions. The most important and very well studied equations are the Korteweg-de Vries equation with serveral of its modifications, the sine-Gordon equation and the nonlinear Schrödinger equation (NLSE). Historically, the first person who observed a solitary wave was the scotsman J.S. Russell [1,2]. He discovered on the Edinburgh-Glasgow channel that a large solitary 'heap of water', as he calls this phenomenon,

moves over a very long distance without been dispersed. The equation of motion to describe these waves in shallow water was first found by D.J. Korteweg and G. de Vries in 1895 [3]. After this it took some time, until 1967, when C.S. Gardener, J.M. Greene, M.D. Kruskal and R.M. Miura [4,5] showed that the Korteweg-de Vries equation can be solved analytically with the so-called inverse scattering theory (IST). Moreover, it was also possible to solve the sine-Gordon equation and the NLSE with the aid of the same method [6–8].

In the present paper we study the NLSE which appears with its variants in problems drawn from disciplines as diverse as optics, solid state, particle and plasma physics. There, the NLSE describes phenomena such as modulational instability of deep water waves [9], propagation of heat pulses in anharmonic crystals, helical motion of very thin vortex filaments, models of protein dynamics [10], nonlinear modulation of collisionless plasma waves [11], transmission of pulses through junctions in optical fibers [12–14], and self-trapping of light beams in optically nonlinear media [15,16]. In the last decade the optical communication via solitons has become a field of special interest [17–20]. In all these applications, the main interest is due to the fact that the NLSE is the most fundamental model which describes the interplay between weak dispersion and nonlinearity for a wave envelope. The existence of soliton solutions is one consequence of this. These are solitary waves with well defined pulse-like shapes and remarkable stability properties [21].

A great deal of current interest is directed to the question how solitons behave under the influence of external perturbations [15,22–27]. The perturbations describe e.g. various dissipative effects, inhomogeneities of a medium or effects of external fields. They can be naturally divided into two classes: Hamiltonian and dissipative. Unfortunately, most of them destroy the integrability of the NLSE. But in many cases, the perturbations are small and the techniques of analytical perturbations theory can be applied to extract some results. Perturbation-induced effects are of interest mainly because they represent physical phenomena that cannot be comprised by exactly integrable models.

Here we shall limit ourselves to such perturbations which can be described by potentials. They preserve the Hamiltonian structure of the NLSE [11], but not its complete integrability. More precisely, we shall consider the one-dimensional NLSE with external potentials which are constant outside a finite interval. Thereby we emulate the effect of an interface with finite width between two different media in which the solitons have different characteristics. We study initial conditions consisting of one single soliton which moves towards the interface. There it will interact and, in general, it will not just be transmitted or reflected. Instead, we expect that the soliton will also undergo inelastic scatterings where it breaks up either into several solitons or into nonsolitary waves, or both.

This problem has been studied previously by several authors. While perturbative approaches were used in [15,16,25,28], straightforward numerical integrations were made in [26,29,27]. Both approaches showed that the soliton behaves just like a Newtonian particle if the force created by the potential is sufficiently weak. This is to be expected, but the problem what happens when the force is strong was not studied extensively. The problem with discontinuous potentials is considered in [30,31], where the main interest was broken conservation laws and soliton tunneling. In [32] the authors have studied the behavior of the soliton scattering at a potential ramp only qualitatively. The main goal was the successful application of higher order symplectic integrators to the NLSE. The spatial inhomogeneity considered in [16] was more complicated, because the authors allowed also a discontinuity in the nonlinear part. That lead to a different behavior of the scattered solitons.

It is one purpose of the present paper to study the potential ramp [28,33] in a more quantitative and systematical way. The main reason to investigate this kind of external potential was the fact that it reveals a very interesting feature. Namely, while for most parameter values of the slope and the hight of the potential the soliton behaves as expected in a "particle-like" manner, for special sets of parameters the soliton shows decidedly inelastic properties. In particular, the nonlinear reflection and transmission coefficients of the mass and of the energy are shown to possess windows of behavior that are quite counter-intuitive at first sight. We find that as the width of the potential ramp is varied, the transmission coefficient abruptly drops from a finite non-zero value to near zero and then just as abruptly back to a value near 1. This feature does not disappear if one smoothes the potential. Only for very smooth potentials the behavior of the soliton equals more and more that of a Newtonian particle in an equivalent potential. First we have compared some of our numerical results for the flat potential step with predictions by perturbation theory. They agree very well in the expected validation range.

We also have extensively discussed the influence on the soliton parameters (amplitude and velocity) during the scattering process. There we come to the conclusion that the solitons escaping in both regions after the scattering are "amplified solitons". These are solitons whose amplitude is multiplied by some constant factor. Their behavior was studied by Kath and Smyth [34] who derived a formula to predict the amplitude oscillation period depending on the soliton parameters. This formula is applied to our data and is in quite good agreement with them.

This article is organized as follows. In the next section we briefly summarize some basic relations and equations concerning the soliton solutions of the NLSE and introduce our problem. A detailed discussion of the transmission coefficients is made in Sec. 3. There some simulations are compared with results from the perturbation analysis, as far as this is possible within its

validity range. In Sec. 4 we take a closer look at the shape of the soliton after it is scattered at the inhomogeneity. An amplified soliton ansatz is made and the parameters of the corresponding solitary wave are determined. A summary and outlook is given in Sec. 5. In the appendix the applied integration method (symplectic integrators) is shortly described. The advantage over the other explicit integration schemes commonly used in this field, such as Runge-Kutta or predictor-corrector methods, is explained.

2 The NLSE soliton solution

Using appropriate units, we can write the NLSE as

$$i\frac{\partial\Psi(x,t)}{\partial t} = -\frac{1}{2}\frac{\partial^2\Psi(x,t)}{\partial x^2} \; - \; |\Psi(x,t)|^2\Psi(x,t) + V(x)\;\Psi(x,t), \qquad (1)$$

where $V(x)$ is the external potential. We shall use for the latter a piecewise linear ansatz, with $V(x) \equiv 0$ for $x < 0$, $V(x) \equiv V_0 > 0$ for $x > x_0 \geq 0$, and linearly rising for x between 0 and x_0,

$$V(x) = \begin{cases} 0 & : \quad x < 0 \\ xV_0/x_0 & : \quad 0 \leq x < x_0 \\ V_0 & : \quad x \geq x_0 \end{cases} . \qquad (2)$$

We call the negative x-axis region I, while region II is the region $x > 0$ (where $V(x) > 0$).

The NLSE with the perturbation (2) is not completely intergrable. But for a constant potential V_0 it is, and the soliton solutions of Eq.(1) form a two-parameter manifold (apart from translations). Taking as parameters the velocity v and the amplitude a, these solutions read [35]

$$\Psi(x,t) = \frac{a}{\cosh[a(x-vt)]} e^{i\{vx+[(a^2-v^2)/2-V_0]t\}} . \qquad (3)$$

We denote the velocity of the incoming soliton as v_0. Using a suitable rescaling of x, t and Ψ, we can always choose its amplitude as $a_0 = 1/2$, without loss of generality.

Among the infinitely many conserved quantities (for $V(x) = \text{const!}$) [25], the following three are of particular interest:

(i) the mass or "number of quasi-particles"

$$N = \int |\Psi|^2 \, \mathrm{d}x \,, \tag{4}$$

which is conserved due to phase invariance;

(ii) the energy

$$E = \int \left(\frac{1}{2} \left| \frac{\partial \Psi}{\partial x} \right|^2 - \frac{1}{2} |\Psi|^4 + V(x) \, |\Psi|^2 \right) \, \mathrm{d}x \,, \tag{5}$$

which is conserved due to time invariance;

(iii) and the momentum

$$P = \frac{1}{2i} \int \left(\Psi^* \frac{\partial \Psi}{\partial x} - \Psi \frac{\partial \Psi^*}{\partial x} \right) \, \mathrm{d}x \,, \tag{6}$$

which is conserved due to translation invariance.

For the soliton given by Eq.(3) this yields

$$N = 2a \,, \tag{7a}$$
$$P = vN \quad \text{and} \tag{7b}$$
$$E = (v^2/2 - a^2/6)N + \langle V \rangle N \,, \tag{7c}$$

where the average over $V(x)$ is taken with weight $\propto |\Psi|^2$ as indicated by Eq.(5).

In the cases where the soliton retains its shape, the motion of the soliton can be understood as that of a Newtonian particle moving in the presence of an effective potential [36]. This assumption is valid when the force created by the external potential is sufficiently weak. In our case this is true when the local disturbance is small, i.e. $V_0 \ll K_0$ or when $x_0 \gg V_0$ in our case. Then we can apply Ehrenfest's theorem to get the effective potential describing the motion of the Newtonian particle with mass $m = 2a_0 = 1$ and initial velocity v_0. Thus, in the case where the potential is much smaller than the kinetic energy of the particle ($V_0 \ll K_0, K_0 = v_0^2/2$) we expect transmission with a final velocity $v_{II,\mathrm{out}} = \sqrt{v_0^2 - 2V_0}$. This follows from the energy conservation law and the assumption that the soliton remains entire and no radiation is emitted. This also predicts that there is no transmission if $v_0 < \sqrt{2V_0}$ (i.e., $K_0 < V_0$) and $x_0 \gg V_0$. But we will see that this is more or less the exception in our simulations and the true behavior will lead to unexpected windows in the transmission coefficients.

To get some more insight into the problem, let us first look at the motion of a Newtonian particle with a shape $|\Psi(x,0)|^2$ in a potential (2). We define the

centre of mass of the extended particle

$$z(t) = \frac{1}{N} \int_{-\infty}^{\infty} \mathrm{d}x \; x|\Psi(x,t)|^2 \tag{8}$$

and derive an effective potential according to which the centre of mass is moving. Starting from the equation of motion we get:

$$\begin{aligned} \frac{d^2z}{dt^2} &= -\frac{1}{N} \int_{-\infty}^{\infty} \mathrm{d}x \; \frac{dV(x)}{\mathrm{d}x} |\Psi(x,t)|^2 \\ &= -\frac{1}{2a} \int_{0}^{x_0} \mathrm{d}x \; \frac{V_0}{x_0} |\Psi(x,t)|^2 \,, \end{aligned} \tag{9}$$

where we have chosen the potential from Eq. (2). While this is still exact for solitary waves, we now approximate the wave function by an unperturbed soliton centered at $z(t)$. The shape of the soliton is then given by

$$|\Psi(x,t)|^2 = \frac{a^2}{\cosh^2[a(x - z(t))]} \,. \tag{10}$$

We are aware that this assumption is valid only if the local derivative of the potential is very small.

From the Eqs.(9) and (10) we can derive the effective potential

$$V_{\text{eff}}(z) = \frac{V_0}{x_0} \left[\ln \left(\frac{\cosh(az)}{\cosh(a(z - x_0))} \right) + \frac{x_0}{2} \right] \tag{11}$$

according to which the centre of mass of a soliton (3) is moving. In the limit $ax_0 \gg 1$ one sees that $V_{\text{eff}}(z) \to V(z)$. In the upper limit $x_0 \to 0$ in which the potential becomes a step function the effective potential takes the form

$$V_{\text{eff}}(z) = \frac{V_0}{2} (\tanh(az) + 1) \,, \tag{12}$$

which agrees with the potential derived by Nogami and Toyama [29].

As one can easily see these functions are smooth sigmoids in contrast to $V(x)$. Due to this it is possible that the soliton's centre of mass penetrates into the region *II* (i.e., where $z > x_0$) although $V_0 > K_0$.

Because of the fact that the effective potential has no local minima the soliton cannot be at rest at any place (provided that $v_0 \neq 0$). This statement does not hold if one also allows a change in the nonlinear term at the inhomogeneity [15]. Then it is possible that the soliton is trapped in the vicinity of the inhomogeneity.

3 Transmission and reflection coefficients

Within our simulations we have intensively studied the transmission coefficients of the mass, the momentum, and the energy. We found that they strongly depend on the geometry of the external potential. Especially the slope of the ramp has a very strong influence on them, which is not expected for the equivalent particle method [36]. For the integration we used a fourth order symplectic integration algorithm [32] which is described in the appendix.

We measured the mass N_i and the energy E_i in each region ($i = I, II$) separately. Notice that N and E are conserved even in the presence of a nonconstant potential [30]. Thus, they are of special importance among the infinite numbers of conserved quantities in the case where the potential is constant [25]. Accordingly, we can define two sets of transmission and reflection coefficients. We call them T_N, R_N and T_E, R_E,

$$T_N = \frac{N_{II}}{N} , \qquad R_N = \frac{N_I}{N} = 1 - T_N \tag{13}$$

and

$$T_E = \frac{E_{II}}{E} , \qquad R_E = \frac{E_I}{E} = 1 - T_E . \tag{14}$$

A physical interpretation of T_N can be the following: if N is the number of quasi-particles of the incoming soliton, then is T_N the quantity of quasi-particles penetrating the potential; resp. is T_E the energy of these quasi-particles.

Another quantity of interest is the momentum. It is only conserved for a constant potential; otherwise the translation invariance is broken. Nevertheless the momentum of the transmitted and reflected wave can be defined in the same way

$$T_P = \frac{P_{II}}{P} , \qquad R_P = \frac{P_I}{P} . \tag{15}$$

Due to nonconservation, in general we have $T_P + R_P \neq 1$.

All these coefficients are functions depending on the incident velocity v_0 of the soliton, the height V_0 and the length x_0 of the potential ramp. Our main interest lays in the detailed dependence on these parameters. Thus, we numerically evaluate the coefficients for a few initial velocities of the soliton varying the length and the height over a wide range.

Primarily, we will study these coefficients in a parameter range where the perturbation approach is not valid. Only very few works in this field have dealt with perturbations which are of the same order as the energy of the soliton. Up to now the only way to get some insight is to simulate the NLSE numerically.

In the following simulations we used $\Delta t = 0.005, \Delta x = \frac{\pi}{16} \approx 0.2$, and $a_0 = 1/2$. Hence the initial soliton takes the form

$$\Psi(x, t = 0) = \left\{2 \cosh[\tfrac{1}{2}(x - x_{\text{off}})]\right\}^{-1} e^{i\, v_0\, x}\,, \tag{16}$$

where the offset x_{off} is the position of the soliton at $t = 0$. The kinetic energy of the soliton is, according to Eq. (5), $K_0 = v_0^2/2$.

In addition to the transmission and reflection coefficients we also registered all local maxima of $|\Psi(x)|^2$ with $|\Psi(x)|^2 > 1/3000$. The threshold was chosen in such a way that no essential information is lost, but small radiation and the noise which is produced due to the numerical integration are not taken into account.

3.1 Transmitted mass and energy

3.1.1 Potential step

Let us first examine the potential step ($x_0 = 0$), because there it is possible to compare the numerically measured transmission coefficients with the results calculated by perturbation theory. These calculations are valid only in two situations: when the potential step is very low in comparison to the kinetic energy of the soliton, and when the potential is much higher than the kinetic energy (reflection at a hard wall).

In the first case the soliton is transmitted nearly without loss of radiation. The determination of the transmission coefficient is based on the IST technique using a first order Born approximation. I.e., the velocity of the soliton is assumed to be constant during the scattering process. This is equivalent to the inequality [24]

$$K_0 \gg 8a_0^2|V_0|\,. \tag{17}$$

In order to calculate analytically the transmission coefficient for a single soliton of the perturbed NLSE ($V_0 \ll K_0$)

$$i\frac{\partial\Psi(x,t)}{\partial t} = -\frac{1}{2}\frac{\partial^2\Psi(x,t)}{\partial x^2} \; - \; |\Psi(x,t)|^2\Psi(x,t) + V_0 f(x)\; \Psi(x,t)\,, \qquad (18)$$

we follow the derivation given in [37]. There the authors study a soliton which is scattered at an impurity (f is a Dirac δ-distribution), whereas in our case the function f is the step function

$$\theta(x) = \begin{cases} 0 & : \quad x < 0 \\ 1 & : \quad x \geq 0 \end{cases}. \qquad (19)$$

A calculation with this potential analogous to that in [37] gives a formula for the amount of radiation which is emitted in the backward direction,

$$\hat{R}_N = \int\limits_{-\infty}^{0} \mathrm{d}\lambda\, n_{\mathrm{rad}}(\lambda)\,, \qquad (20)$$

and the energy of that radiation,

$$\hat{R}_E = \int\limits_{-\infty}^{0} \mathrm{d}\lambda\, 4\lambda^2\, n_{\mathrm{rad}}(\lambda)\,, \qquad (21)$$

Here $n_{\mathrm{rad}}(\lambda)$ denotes the total density of linear waves emitted by a soliton during the scattering,

$$\begin{aligned} n_{\mathrm{rad}}(\lambda) = & \frac{\pi V_0^2}{v^4}\; \beta^2(\lambda)\, \mathrm{sech}^2\left[\frac{\pi}{av}\left(2\lambda^2 + \frac{a^2}{2} - \frac{v^2}{8}\right)\right] \qquad (22) \\ & \times \int\limits_{-\infty}^{\infty}\mathrm{d}x \int\limits_{-\infty}^{\infty}\mathrm{d}x'\, f(x)\; f(x')\; \exp[i\beta(\lambda)(x-x')]\,, \end{aligned}$$

where

$$\beta(\lambda) = \frac{4}{v}\left[\left(\lambda + \frac{v}{4}\right)^2 + \frac{a^2}{4}\right].$$

The analytic calculation yields for the step function

$$\hat{R}_N = \frac{\pi V_0^2}{v^4} \int\limits_{0}^{\infty}\mathrm{d}\lambda\, \mathrm{sech}^2\left[\frac{\pi}{av}\left(2\lambda^2 + \frac{a^2}{2} - \frac{v^2}{8}\right)\right], \qquad (23)$$

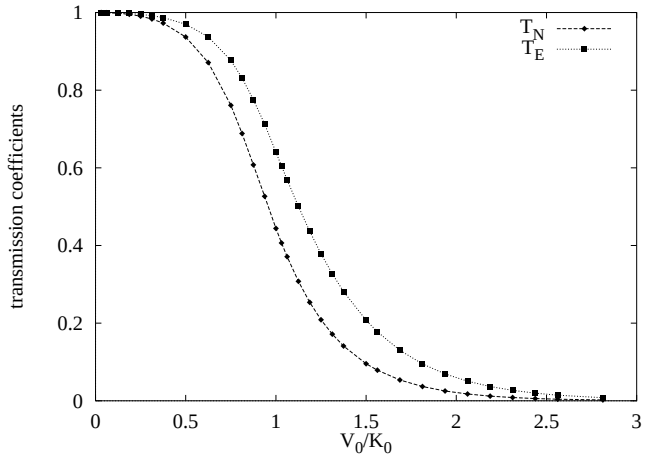

Fig. 1. The transmission coefficients T_N and T_E vs. V_0/K_0 with fixed $x_0 = 0$ and $v_0 = 0.8$. Errors are smaller than the symbols. The continues lines are drawn for guiding the eyes.

and

$$\hat{R}_E = \frac{\pi V_0^2}{v^4} \int_0^\infty \mathrm{d}\lambda \, 4\lambda^2 \, \mathrm{sech}^2 \left[\frac{\pi}{av} \left(2\lambda^2 + \frac{a^2}{2} - \frac{v^2}{8} \right) \right] . \tag{24}$$

Inserting the parameters of the initial soliton ($v_0 = 0.8, a_0 = 0.5$) and then calculating the integral numerically (using *Maple V*) it gives the simple equations $\hat{R}_N \simeq 1.31 V_0^2$ and $\hat{R}_E \simeq 0.71 V_0^2$. This corresponds to a transmission coefficient for the mass

$$\hat{T}_N = 1 - \hat{R}_N \simeq 1 - 1.31 V_0^2 \tag{25}$$

and for the energy

$$\hat{T}_E = 1 - \hat{R}_E \simeq 1 - 0.71 V_0^2 \, . \tag{26}$$

The quanitative behavior of the transmission coefficients measured from our simulations is shown in Fig. 1. The height of the simulated potential step ranges from almost 0 to about three times the kinetic energy of the soliton. The transmission coefficients fill monotonously the range from 1 to 0. We want to point out that the value of T_E is always larger than T_N. This is due to the fact that the kinetic energy is larger than the internal binding energy of the soliton ($3v_0 > a_0$).

In Fig. 2 the result of perturbation theory (25) and (26) is compared with our numerically measured transmission coefficient T_N for small parameters

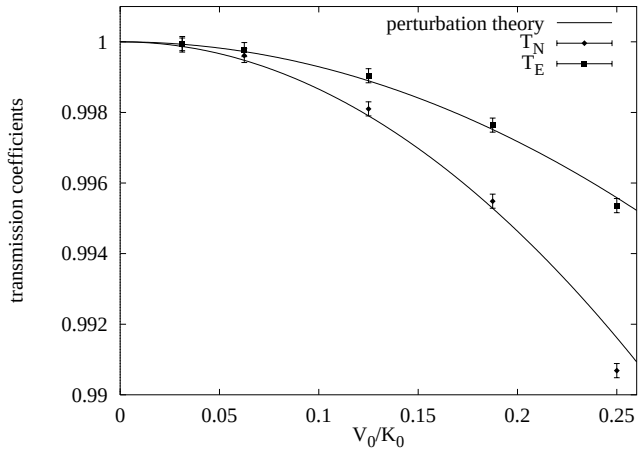

Fig. 2. Comparison between the measured transmission coefficients T_N and T_E and the perturbation theory result $\hat{T}_N = 1 - 1.31V_0^2$ and $\hat{T}_E = 1 - 0.71V_0^2$, which is expected to be valid for $V_0/K_0 \ll 1/2$.

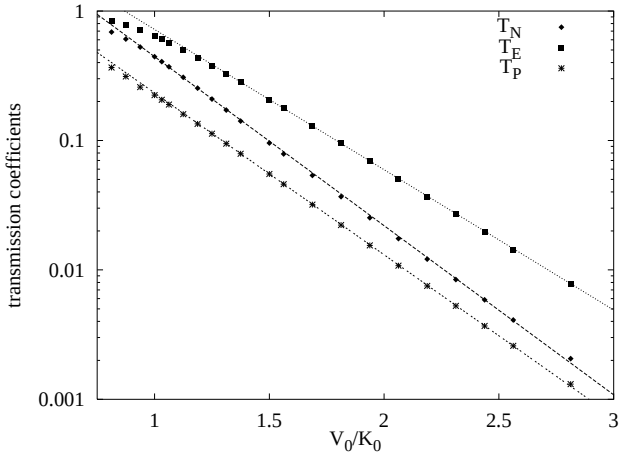

Fig. 3. The transmission coefficients $T_N(\blacklozenge)$, $T_E(\blacksquare)$, and $T_P(*)$ vs. V_0 as in Fig. 1 in a logarithmic scale. An exponential function is fitted to each set of the data (points) to indicate its behavior for large values of V_0/K_0.

V_0. Due to (17) we expect that the perturbation theory is valid in a range $V_0/K_0 \ll 1/2$ in the present case. In fact, one sees a rather good agreement between the data and the first order perturbation theory for low step heights. The discrepancy for larger perturbations ($V_0/K_0 > 0.25$) indicates that higher order perturbation theory would be necessary to predict the transmission of the soliton in this region more precisely. One has to bear in mind that the perturbation analysis assumes that the initial soliton does not break up and no soliton is reflected.

In the opposite case, where the soliton is reflected at very high potential

steps ($V_0 \gg K_0$), we find an exponential decay of the transmission coefficients (see Fig. 3). All three transmission coefficients (T_N, T_E, and T_P) show this exponential decay for $V_0 > K_0$. The exponential functions plotted in Fig. 3 are fitted by hand. This simple behavior strongly suggests that one should be able to derive it analytically. Up to now we did not yet succeed, but we are still working on this problem. Intuitively it is clear that the higher the potential is the less quasi-particles penetrate into region *II*. This amount of quasi-particles decreases exponentially with the penetrating depth of the soliton, because the tail of the soliton decays exponentially. Therefore the amount of quasi-particles "pushed" into and staying in region *II* decreases exponentially with increasing V_0.

3.1.2 Potential ramp

Let us now study potential ramps for positive values of x_0, i.e. potential ramps with finite slopes. Our data show unambiguously that the slope has a strong influence on the scattering process. In the equivalent particle method [36], where the soliton is treated like a classical Newtonian particle with mass N and kinetic energy K_0, one would expect that the transmission coefficients remains constant when changing the length of the ramp. This would be due to the constant difference $V_0 - K_0$. But it turns out that this simple picture is not true in our case. Bearing in mind that the transmission coefficients for a Gaussian wave packet of the linear Schrödinger equation being scattered at a potential ramp shows a dependence of the slope, too, this is not that remarkable. But the windows of reflection are.

In figure 4 the transmission coefficient T_N are plotted for different slopes and heights of the ramp. A similar figure with less complete data was already shown in Ref.[38]. In the following we will show mainly data for a initial velocity $v_0 = 0.8$ without loss of generality. We also have simulated different initial velocities v_0 and have found very similar results.

Let us first shortly recapitulate the observations found in Ref. [38] concerning the global behavior of the transmission coefficient. After that we want to discuss the windows of reflection in a more detailed manner.

The obvious stucture one observes is that the curves for $V_0 > K_0 = 0.32$ tend to 0 if $x_0 \to \infty$, while those for $V_0 < K_0$ tend to 1 in this limit. This indicates that the equivalent particle method is valid in the limit of very flat ramps. If the kinetic energy of the soliton is smaller than the potential height, it will be totally reflected; otherwise it will be totally transmitted. Simulations with still flatter ramps, e.g. $x_0 = 100$ (not shown here), show that the transmission coefficients are equal to 1 resp. 0 within the error bars.

Another property is the nonmonotonic behavior of the transmission coefficients

at steep ramps. All curves $K_0 \leq V_0$ show a global maximum at $x_0 \approx 3$. If V_0 is decreased below K_0, the absolute maximum is reached in the limit $x_0 \to \infty$ (that is 1), but there is still a local maximum as long as $V_0 \gtrsim 0.31$. At some threshold this local maximum transforms into a shoulder. In Fig. 4 this threshold is at $V_0 \approx 0.31$ for T_N, while it happens at $V_0 \approx 0.3$ for T_E [38]. For all values of $V_0 \lesssim 0.31$ the position of this bump nearly stays at the same place. Simulations with different initial velocities ($v_0 = 0.2, 0.6$) likewise show such a maximum resp. shoulder at $x_0 \approx 3$. The fact that the maximum resp. the shoulder is located at a length of the ramp which is roughly equal to the width of the soliton, strongly suggests that this is a nonlinear resonance effect. A very similar behavior of the reflection coefficient was found by Yu.S. Kivshar *et al.* [37] for solitons scattered by a single impurity.

Besides the global maximum, the curves for high potentials ($V_0 \geq 0.36$) show a slight shoulder at $5 < x_0 < 10$. This shoulder gets more and more pronounced if V_0 is decreased towards the magnitude of the kinetic energy ($V_0 = 0.33$). At the same time its position is shifted towards flatter slopes ($x_0 \approx 7 \to 12$) and the shoulder becomes sharper. In case the height reaches K_0 ($V_0 = 0.32$) this shoulder is a dominating feature.

Decreasing the potential further (below K_0, but still above some threshold $V_{0,c}$), this shoulder continues to become sharper and more pronounced. Indeed, it develops into a peak and the transmission coefficients begin to grow

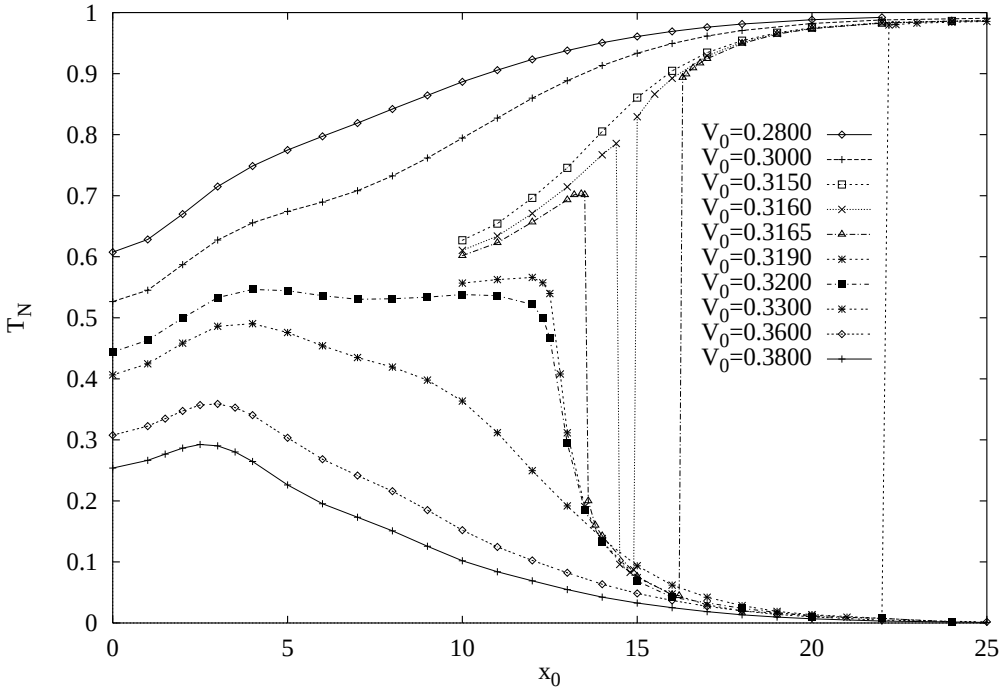

Fig. 4. The transmission coefficient T_N vs. x_0 for different potential heights and $v_0 = 0.8$.

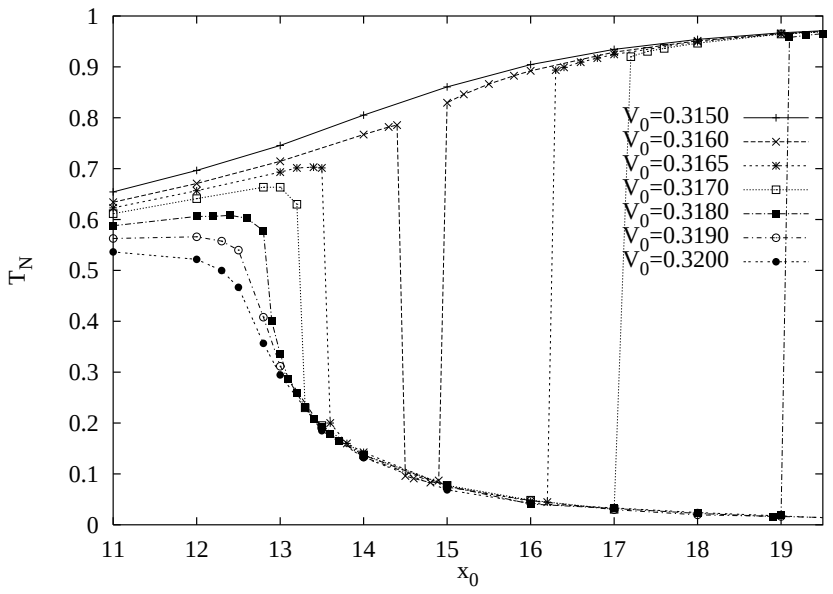

Fig. 5. The transmission coefficient T_N vs. x_0 as in Fig. 4, but displaying additional curves revealing windows of reflection ($0.315 \leq V_0 \leq 0.32$) with higher resolution.

with x_0 before they rapidly drop to join a common curve. This curve seem to be independent of V_0 within the interval $V_{0,c} < V_0 < K_0$. But the transmission coefficients do not stay on this common curve as we increase x_0 further. We observe that the limit value for very flat slopes is not reached smoothly. Instead, the transmission coefficients jump back—instantaneously within our resolution—to values ≈ 1. The values of x_0, where these jumps happen, seem to diverge when $V_0 \to K_0$ from below.

As V_0 is decreased further, we reach a value $V_{0,c} = 0.3155 \pm 0.0005$ where the window of small transmission coefficients disappears. As $V_{0,c}$ is reached from above, the locations of the downward jump and of the upward jump both tend towards $x_{0,c} \approx 14.7$. At this point, both jumps seem to be instrumentally sharp. For $V_0 > V_{0,c}$ only the second jump retains this sharpness. For $V_0 < V_{0,c}$, no trace of this singular behavior is left, and the transmission coefficients rise monotonically towards their asymptotic value 1 as x_0 is increased. An enlargement of the relevant part of Fig. 4, together with some more data, is shown in Fig. 5.

These unexpected and surprising windows of small transmission coefficients were first seen in [38]. This effect is not expected within the picture of the equivalent particle method or within the linear Schrödinger equation. Superficially similar effects have been observed within the SG Eq. [39] and the ϕ^4-model [40]. But there are some fundamental differences to the actual work. These authors have studied the effect of a local and attractive impurity which

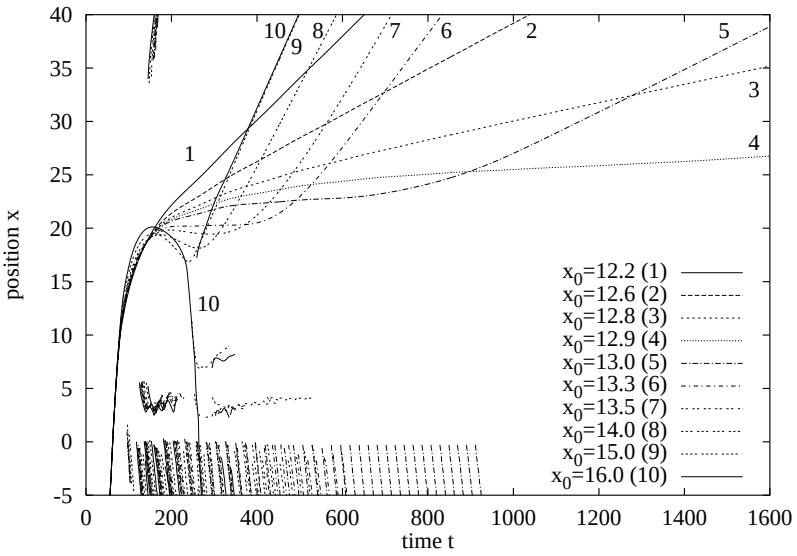

Fig. 6. Time evolution of the local maxima of $|\Psi|^2$ for ten different slopes of the potential ranging from $x_0 = 12.2$ to $x_0 = 16.0$. The initial velocity is $v_0 = 0.8$ and the height of the potential is $V_0 = 0.3180 = 0.99375K_0$. Only the maxima $|\Psi|^2 > 1/3000$ are plotted, and only the most important maxima are labeled. The calculation was done on a lattice with 8192 sites, discretization width $\Delta x \approx 0.2$ and integration step $\Delta t = 0.005$.

is such that the soliton can be captured, and the energy is stored in an internal mode. This leads to sharp resonance frequencies. Another difference is that the soliton is unbreakable in [39,40]. Thus, in contrast to our system, the soliton is either reflected or transmitted or captured (in a state oscillating around the impurity) and does not emit radiation. The authors of [39,40] observe that the soliton may be reflected by the attractive impurity when its velocity lies in one of several windows. Within our resolution we find only *one* window, where the soliton is reflected instead of being transmitted. There are no indications for further windows of reflection.

To understand this phenomenon in more detail, we first try to get some more insight by looking at the evolution of the wave function. In Fig. 6 we show the local maxima of $|\Psi|^2$ for $V_0 = 0.3180 = 0.99375K_0$. In this diagram one can directly compare the effect of different slopes on the movement of the soliton. Let us begin with the steep ramp $x_0 = 12.2$ (label 1 in the figure). Here the soliton lowers its speed while it climbs the potential ramp. At the same time radiation is emitted in the forward and backward direction. The biggest amount of radiation is emitted at the lower part of the ramp and immediately forms a new soliton escaping in the backward direction. The slowing down process continues until $t \approx 350$ and is accompanied with loss of radiation in the backward direction. After that the soliton moves with constant velocity

in the forward direction. But its mass has shrunk to roughly 60% of its initial mass.

Flattening the slope of the ramp, the velocity of the transmitted soliton reduces continuously. Whereas its mass decreases only slightly. If the slope is $x_0 = 12.8$ the soliton interacts with the ramp until $t \approx 1000$. This corresponds to a distance $x \approx 18$ between the maximum of the soliton and the upper edge of the ramp. The same holds for the steeper slopes described above.

Flattening the slope a tiny bit more ($x_0 = 12.9$) the soliton nearly stops after penetrating in to region *II*. It takes very long ($t \approx 1400$) until the soliton decides in what direction to move on. One consequence is that more radiation is emitted into region *I* while the soliton interacts with the inhomogeneity. The mass shrinks to roughly 40%, and it takes until $t \approx 2700$ that the soliton accelerates to full speed (not shown in Fig. 6).

This behavior changes if the slope is again only slightly flatter. For $x_0 = 13.0$ the soliton moves with constant positive velocity already at $t \approx 1100$. But its loss of mass due to radiation is much higher. The transmitted soliton has only roughly 33% of its initial mass. This loss creates *more than one* new soliton and nonsolitary waves escaping from the ramp in the backward direction. It is hard to distinguish between solitons and nonsolitary waves here, because the amplitudes are small and furthermore the amplitude oscillates with a very low frequency, which makes it hard to identify them as solitons. [1] One should notice, that nonsolitary waves are created near the lower edge of the ramp at least until $t \approx 900$. The other waves are not plotted, because their amplitude is less than 1/3000. As one can see from Fig. 7 the transmitted soliton continuously loses mass while it interacts with the potential ramp. This happens until it leaves the upper edge of the ramp and moves with constant speed again.

If one looks closer at the traces of the transmitted soliton in Fig. 6 one observes small bends at times $t \approx 200$, 350, 500 and 650. It looks as if the soliton's maxima are oscillating around a true trace. This frequency corresponds exactly to the oscillation period of the amplitude of those solitons. More precisely this means that the apparent bend in the trace occurs when the transmitted soliton is maximally sharp. This can be explained in the following way: the soliton is stretched when it climbs up the ramp, which causes the amplitude to be reduced. Thereby it becomes asymmetric as one can see in Fig. 2 of Ref. [38] and its tail stays on the ramp for a long time. During that time the pulsating soliton still interacts with the ramp, which causes the oscillations seen in Fig. 6.

While decreasing the slope of the ramp more and more the mass of the trans-

[1] The reader is refered to section 4.1 where the amplified solitons are discussed in more detail.

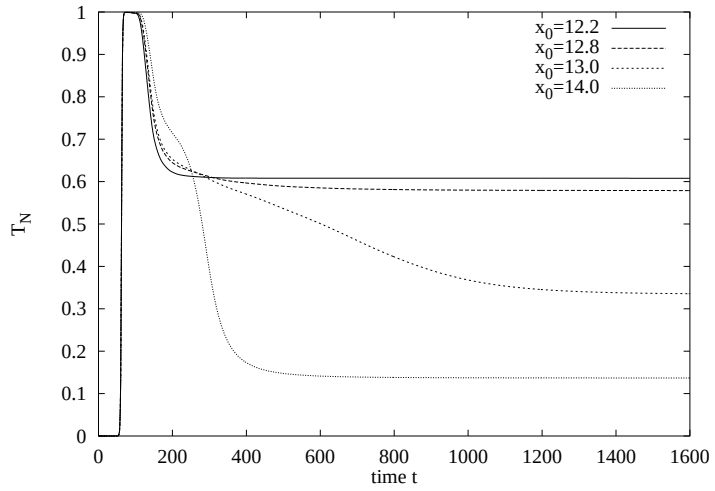

Fig. 7. Time evolution of the transmission coefficient T_N of four representative values of x_0 (12.2, 12.8, 13.0 and 14.0). The height of the potential is $V_0 = 0.3180 = 0.99375K_0$ as in Fig. 6

mitted soliton resp. solitary wave drops rapidly but continuously to $\approx 10\%$ (see Fig. 7). This is the reason why the speed of the soliton increases at the same time. For slopes $13.5 < x_0 < 15.0$ the movement of the penetrating soliton is not monotonical. After it has come to a stop at $t \approx 200$ it moves back before it stops again and escapes in the forward direction. E.g. let us look at the situation with $x_0 = 14.0$: at $t \approx 200$ the soliton becomes wider, which can be concluded by comparing the oscillations of the other traces shown in Fig. 6. Due to this broadening its maximum is shifted towards region I. During this process some of its mass is pushed down the ramp into region I. That can be concluded from Fig. 7 where the curve shows a drop at $T \approx 200$, after it had seemed to converge to a value larger than that for $x_0 = 12.8$. After some part of the soliton has separated from the bulk it accelarates away from the ramp while it contracts again.

For $x_0 = 16.0$ the soliton penetrates into region II, but is reflected at the top edge of the ramp. This is consistent with the collective-coordinate description (see Eq.(11)). The reflected soliton consists of roughly 96% of the initial mass. This scenario holds for flatter slopes, too, until $x_0 = 19.1$. There the soliton is transmitted with roughly 95% of its initial mass and only few radiation is emitted.

For heights V_0 close to $V_{0,c}$ the first jump becomes sharper and finally as sharp as the second one.

As already pointed out in our previous work [38] the second upward jump can be explained easily: If there were no radiation (as is the case for $x_0 \to \infty$) the

energy of the soliton would be conserved, and the threshold for transmission would be strictly at $V_0 = K_0$. But for finite x_0, the radiation implies that the soliton has lost energy when it reaches the upper end of the ramp, and it needs $K_0 > V_0$ to be transmitted. Thus there is a range $K_0 - \delta(x_0) < V_0 < K_0$ where the soliton is reflected. Since the soliton moves very slowly near the upper egde of the ramp for $V_0 \approx K_0 - \delta(x_0)$, the dependence of the transmission coefficients on the amount of radiation (and thus also on x_0) is extremely sharp. To be more quantitative, let us consider $V_0 = 0.3190$. Here, the second jump (from nearly total reflection to nearly total transmission) occurs at $x_0 = 22.1 \equiv x_c$. At this slope, T_E jumps from 0.0093 to 0.9837, while T_N jumps from 0.0074 to 0.9797. The fact that the soliton is coming to a near stop for $x_0 = x_c + \epsilon$ means that all its energy is potential energy, $E' = N'(V_0 - a'^2/6)$, and the energy difference has gone into radiation. Primes denote here observables at the moment when the soliton stops. If we neglect the forward radiation (which seems to be indeed small according to Figs. 6), we have $N' = T_N$, $E' = T_E E_0$ and $a' = (T_N/2)^2$, and thus $T_E = T_N(V_0 - T_N^2/24)/E_0 = 0.9821$ for $x_0 = x_c$. Comparing this with the measured value 0.9837 we see good agreement.

Within the window of reflection, the time it takes until the point of return is reached is not the same for different slopes. This time becomes larger and larger the nearer the slope is to the border of the window. Indeed, that is true for both borders. The reason for this is that the radiative loss of energy is equal to the difference $K_0 - V_0$. Therefore the velocity of the temporarily transmitted soliton is very close to 0. Thus, the soliton stays during a long time in the vicinity of the egde of the ramp and can interact with it. This means that already tiny amounts of radiation can cause the soliton to turn back into region I. The same argument holds when decreasing the difference $K_0 - V_0$. The smaller it is, the longer it takes until the soliton has decided whether to pass the potential ramp, or to fall back into region I.

In order to exclude that the observed feature is due to the non-differentiability of the chosen potential, we have simulated smoother potentials, too. We found that the values of the transmission coefficients change only slightly if one uses instead of potential (2) a more smooth sigmoid. Even the shape of the windows with small transmission are still seen and they stay at the same positions. However, if the potential becomes too smooth (e.g. such as functions like $\tanh(sx)$ with $s < 1$), the soliton behaves as one expects for the equivalent particle method and only very little radiation is emitted.

3.2 Transmitted momentum

Another observable we can look at are the momenta of the reflected and transmitted wave. Although momentum is not conserved for nonconstant potentials,

it is worth to have a closer look at it. If the wave function is only composed of a single soliton, its momentum is directly related to its velocity via Eq.(7b). In order to measure the momentum of one soliton within a system of several nonoverlapping solitons, it is necessary to restict the integration interval (in Eq.(6)) around its position. If we neglect the momentum of the radiation, and if at most a single soliton is emitted in the forward and backward direction, it is sufficient to partition the x-axis into regions I and II. That is what we have done.

As mentioned before, according to the equivalent particle method the transmitted momentum should not depend on the slope of the ramp. But what we observe is different, as already pointed out in the previous section. The global behavior of the transmission coefficient is the same as it is for the transmitted mass and energy. In Fig. 8 we see a (local) maximum at steeper ramps ($x_0 \approx 2-3$), which confirms the claim that this is a nonlinear resonance effect. In the limit $x_0 \to \infty$ the momentum tends to the value one expects for the equivalent particle method. There one assumes that if the soliton is transmitted, it is so without loss of radiation. Due to the conservation of energy the reduced velocity is given by $v_{II,\mathrm{out}}$ in the cases where $V_0 < K_0$. Otherwise the soliton is reflected and the momentum of the transmitted solitary wave tends to zero. Our results agree with this expected behavior for very flat ramps ($x_0 \gg 25$).

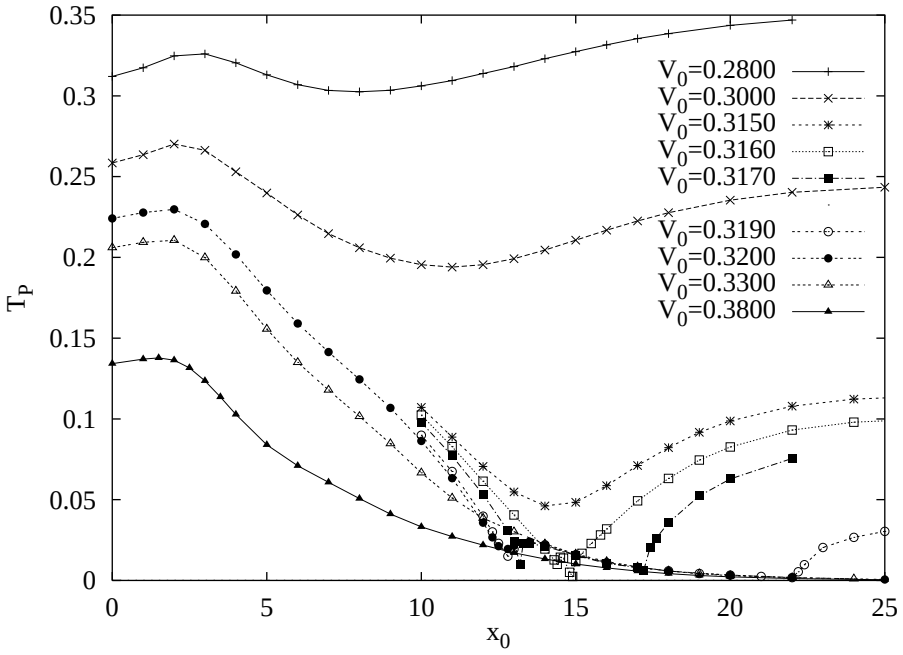

Fig. 8. The transmission coefficient T_P vs. x_0 for different potential heights as in Fig. 4.

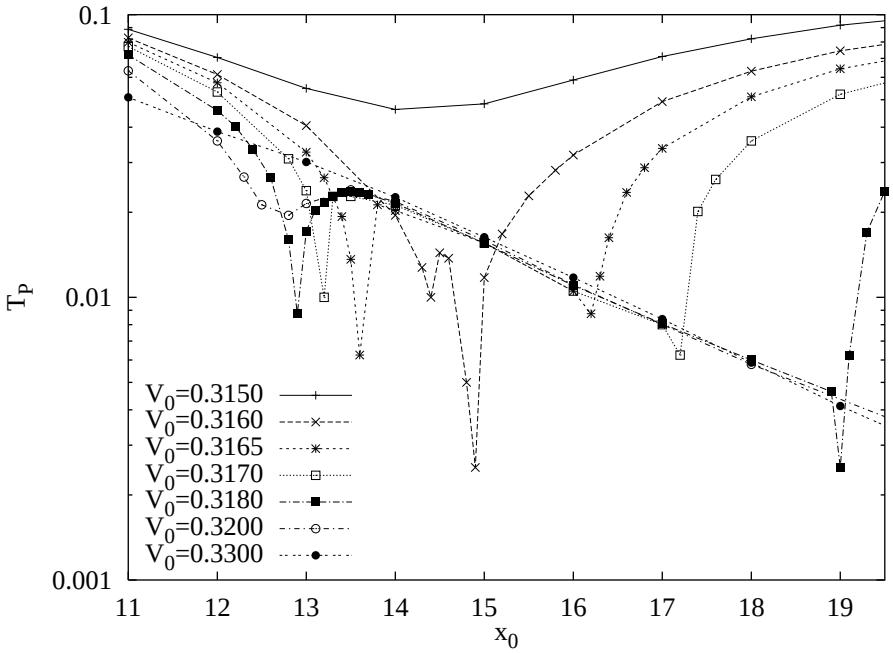

Fig. 9. Enlargement of Fig. 8 on a logarithmic scale. Only transmission coefficients for potential heights $0.3150 \leq V_0 \leq 0.33$ are plotted.

Between the (local) maximum and the limit region ($x_0 \to \infty$) there exists a minimum whose position depends on the height of the potential. For lower heights it is located at steeper ramps ($x_0 \approx 8$). While raising the potential, the minimum gets more pronounced and is shifted to flatter ramps ($x_0 \approx 14$). When the ramp is nearly as high as the kinetic energy of the soliton ($V_0 \lesssim 0.3150$), the values of the transmitted momentum at the minimum is very small and the minimum becomes a dominating feature.

Raising the potential above the threshold $V_{0,c}$ (≈ 0.3155; see subsection 3.1.2) the situation is different. For $V \in [V_{0,c}, K_0]$ the momentum of the transmitted soliton has very sharp minima at both ends of the window of reflection (see Fig. 9). In the interior of the window it is non-zero and decreases exponentially with x_0. The minimum at the upper end of the window tends to zero, and the same holds for the lower end if V_0 is not too close to K_0. But for $V_0 \approx K_0$ ($V_0 \gtrsim 0.3185$) when also the lower end of the window of reflection in Fig. 5 is slightly smoothened, T_P has a smooth dip of finite depth. The larger V_0 is, the smoother the behavior gets. Finally, it vanishes at a height $V_0 > 0.325$. Even the curve for $V_0 = K_0 = 0.32$ shows a smooth dip at $x_0 \approx 12.7$. The cusp at the second edge remains sharp for values $0.3150 < V_0 < 0.3200$. Whereas the first cusp shifts only little from $x_0 = 14.1$ to $x_0 = 12.7$ as $V_0 \to K_0$, the second cusp shifts rapidly from $x_0 = 14.9$ to $x_0 > 22$. For potentials higher than the kinetic energy we do not find any jump from $T_P \approx 0$ to $T_P \approx 1$ at all.

Outside the window but still in its vicinity, the mass of the transmitted soliton stays nearly constant. This leads to the conclusion that the velocity of the transmitted soliton drops to almost zero at the edge of the window. This agrees with the observation made in Fig. 6. The dependence of T_P inside the window is dominated by the mass of the transmitted solitary wave, because its velocity changes only slightly. It is conspicuous that all curves within the window match the exponentially decaying curve for $V_0 = 0.33$. This confirms the conclusion that those transmitted solitary waves are universal in the sense that its mass, energy and momentum are independent of the height of the potential.

4 Shape of the reflected and transmitted soliton

4.1 Description by an amplified soliton ansatz

After the soliton hits the potential ramp, we observed in general that it splits up and creates a transmitted and reflected soliton, which are both accompanied by some radiation (see Fig. 10). This is why we find typically more than a single maximum of $|\Psi(x)|$. Moreover, the heights of these maxima in general are not constant in time, as one would expect for a pure soliton state. Instead, the amplitude of the soliton shows in general marked oscillations (e.g. Fig. 11) which are damped in all cases. In spite of this, the solitons moves with practically constant velocity (see Fig. 10; the small bent lines belong to the maxima of nonsolitary waves).

Damped amplitude oscillations have be observed in connection with 'amplified' solitons. These have been studied analytically and numerically in [41,42,34]. These authors have shown that a soliton whose amplitude is multiplied by some factor relaxes by emitting radiation and by showing damped oscillations of its amplitude. This can be understood by interpreting the initial state as a superposition of a soliton with radiation.

As an example we just show one typical scenario to illustrate the movement and the amplitude behavior of the solitons during the scattering process. Other scenarios are shown in our previous work [32]. Figures 10 and 11 depict the case where the potential is a step function ($x_0 = 0$) and the kinetic energy ($K_0 = 0.32$) is larger than its height $V_0 = 0.3$. In the equivalent particle method one would expect the soliton to move into region *II* and to propagate there with a reduced speed $v_{II,\mathrm{out}}$. But our simulation shows that it breaks up into two solitons with roughly equal heights and with velocities $v = -0.588$ and $w = 0.395$. About half of the mass and three quarters of the energy are transmitted ($T_N = 0.527, T_E = 0.712$).

The loss due to direct radiation is very small. If one inserts the above numbers into Eq.(7c) one finds perfect agreement (discrepancies are $\lesssim 1\%$) [32]. This indicates that radiation in form of nonsolitary waves is small in spite of the wiggles seen in Fig. 11.

Assume now that the wave functions after the interaction can be described in both regions separately by amplified solitons

$$\Psi(x', t' = 0) = \frac{a + \delta}{\cosh(ax')} e^{i\tilde{v}x'} , \tag{27}$$

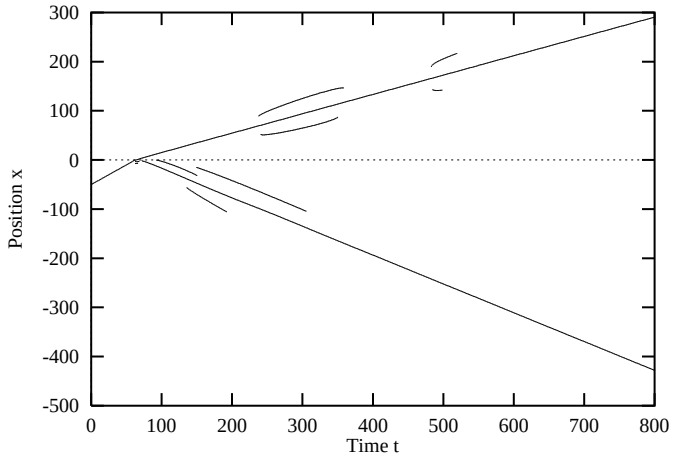

Fig. 10. Time evolution of local maxima of $|\Psi|^2$ for a soliton with incident velocity $v_0 = 0.8$ which is scattered at a potential step with $x_0 = 0$ and height $V_0 = 0.3 = 0.937K_0$. The calculation was done on a lattice with 4096 sites, discretization width $\Delta x = 0.2$ and integration step $\Delta t = 0.005$. The latter parameters are the same for the next figures.

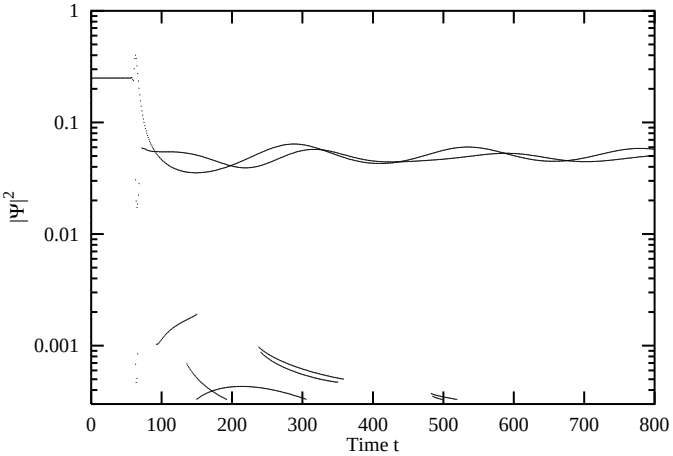

Fig. 11. Time evolution of the height of the maxima shown in Fig. 10. The highest curve belongs to the transmitted soliton, and the second highest to the reflected one. The other maxima presumably are due to the superposition of nonsolitary waves.

where $x' = x - \tilde{x}$ and $t' = t - \tilde{t}$. The parameters $\tilde{x}, \tilde{t}$ specify the location and the time of the interaction and $\tilde{v}$ the new velocity. This function is a soliton whose amplitude is simply multiplied by a factor of $\gamma = 1 + \frac{\delta}{a}$. The long-time asymptotic solution consists just of a soliton. For finite times it shows oscillations [41,42]. They are damped, and the soliton's amplitude tends to

$$\kappa = a + 2\delta \; . \tag{28}$$

The mass of the amplified soliton (27) at time $t' = 0$ is given by

$$N_0 := \int_{-\infty}^{\infty} \mathrm{d}x' \, |\Psi(x', t' = 0)|^2 = 2\frac{(a+\delta)^2}{a} \tag{29}$$

and its maximum is $|\Psi(0,0)| = a + \delta$. Satsuma and Yajima [41] proved that the nonsoliton part of Eq. (27) behaves like an ordinary wave packet and thus decays as $t^{-1/2}$ for $t \to \infty$. The mass of the asymptotic soliton is given by

$$N_\infty := \int_{-\infty}^{\infty} \mathrm{d}x' \, |\Psi(x', t' = \infty)|^2 = 2(a + 2\delta) \, , \tag{30}$$

the difference with Eq. (29) being due to the unobservable radiation.

Now we will use Eqs. (29) and (30) to evaluate the parameters a and δ for the scattered wave functions. Then we will compare the scattering data with a simulation using as initial condition a wave function (27) with the calculated parameters.

The parameters $\tilde{x}, \tilde{t}, \tilde{v}$ have to be chosen in such way that the amplified soliton fits to the scattering data. The velocity $\tilde{v}$ of the scattered soliton can easily be extracted from a plot that shows the time evolution of its maxima (see e.g. Fig. 10). However, the values of $\tilde{x}$ and $\tilde{t}$ are not fixed *a priori*, because they depend on the length of the ramp.

In the case of the potential step ($x_0 = 0$) it is natural to place the interaction point simply at $\tilde{x} = 0$, $\tilde{t} = -x_{\mathrm{off}}/v_0$, where $x_{\mathrm{off}} < 0$ is the position of the soliton at time $t = 0$ (see Eq. (16)). But if $x_0 > 0$ the coordinates of the interaction point are different from those.

To obtain the parameters a and δ of the amplified soliton, the equations

$$N_0 = 2(a + 2\delta + \delta^2/a) \tag{31a}$$
$$N_\infty = 2(a + 2\delta) \tag{31b}$$

have to be solved. Here, N_0 is simply either the transmission or the reflection coefficient, T_N or R_N. The value of N_∞ is taken from plots which show the time evolution of the amplitude. From them it is easy to estimate $\kappa = a + 2\delta$, but the determination of a and δ themselves is less straightforward.

Solving Eqs. (31) we get two sets of solutions:

$$a_{1,2} = N_0 - \frac{N_\infty}{2} \pm \sqrt{N_0(N_0 - N_\infty)}\,, \tag{32a}$$

$$\delta_{1,2} = \frac{N_\infty - N_0 \mp \sqrt{N_0(N_0 - N_\infty)}}{2}\,, \tag{32b}$$

corresponding to initial amplitudes which are larger ($\delta_1 < 0$) resp. smaller ($\delta_2 > 0$) than that of the asymptotic soliton. Also, the period of their oscillations are slightly different.

Unfortunately, those relations do not help to decide which solution, (a_1, δ_1) or (a_2, δ_2), describes the scattered soliton. This can be found out by direct comparison, i.e. numerically, because there does not exist an analytical solution of the NLSE with initial condition (27). As an example, we plotted the two solutions together with the simulations in Figs. 12 and 13, for $v_0 = 0.8$ and $V_0 = 0.3$

As one can clearly see, only the amplified soliton with $a_1 = 0.4894, \delta_1 = -0.1304$ is in good agreement with the data. Both amplified solitons show oscillations with almost the same period as the transmitted one. But the amplitude fits much better for the first solution, and the behavior around the interaction point is much better represented. Also, the side maxima are not that close to the main maximum as it is for the curve with $a_2 = 0.1067, \delta_2 = 0.0609$. All this is an stong indication that the transmitted soliton can be described by an amplified soliton ansatz with solution a_1, δ_1.

Even better fits are obtained in Figs. 12 and 13 if the parameter a is not calculated from Eqs. (32), but is simply chosen as the value $a = a_0 = 0.5$ of the unperturbed soliton. Within errorbars, this is consistent with the above value. The corresponding δ is -0.13575.

For this case ($v_0 = 0.8, V_0 = 0.3, x_0 = 0$) the interaction of the incoming soliton with the potential can be interpreted in the following manner: the soliton with amplitude 0.5 interacts with the potential inhomogeneity ($x_0 = 0$). The main part ($T_E \approx 0.7$) is transmitted, and the remaining part is reflected. Most of the radiation is emitted in the backward direction. Due to the birth of a second soliton the amplitude of the initial soliton is reduced by δ. This new state of the wave function is not a pure soliton any more. Thus, the amplitude decreases further and begins to oscillate in the manner seen in the figures. The reflected wave also forms such an amplified soliton. In addition, radiation is

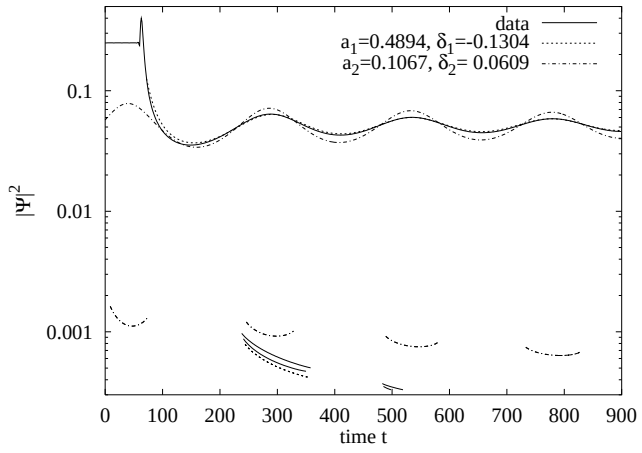

Fig. 12. Comparison between the amplitudes of the two simulated solutions $a_1 = 0.4894 \pm 0.0400$, $\delta_1 = -0.1304 \pm 0.0200$, $a_2 = 0.1067 \pm 0.0150$, $\delta_2 = 0.0609 \pm 0.0070$, and the transmitted soliton, Fig. 11) with the parameters $v_0 = 0.8, x_0 = 0, V_0 = 0.3$.

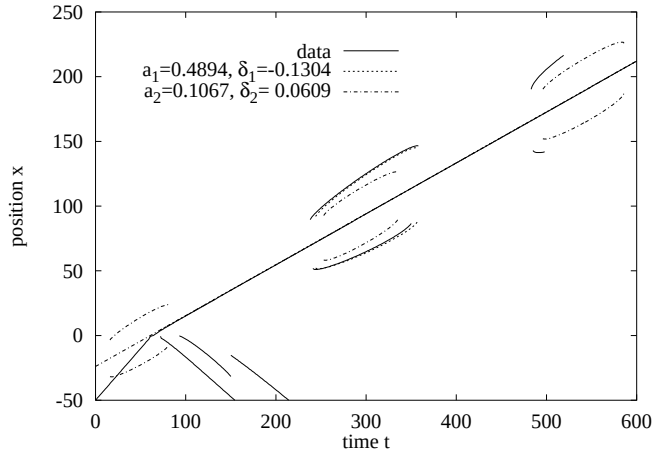

Fig. 13. Comparison between the position of the local maxima of the two simulated solutions and the transmitted soliton as in Fig. 12.

created as seen from the various decreasing and non-oscillating side maxima.

For flatter slopes of the ramp, amplified solitons fit well for times t' larger than one oscillation period of the amplitude. The early stages of the interaction can not be reproduced with this ansatz. In our simulations we observed that the amplitude oscillation is slightly compressed horizontally while the soliton is located in the rising part of the potential. This might be because of the transfer of energy into the radiation.

The amplitude oscillations for the reflected soliton are less easy to compare. This comparison is possible for very steep ramps and rather high potentials. In

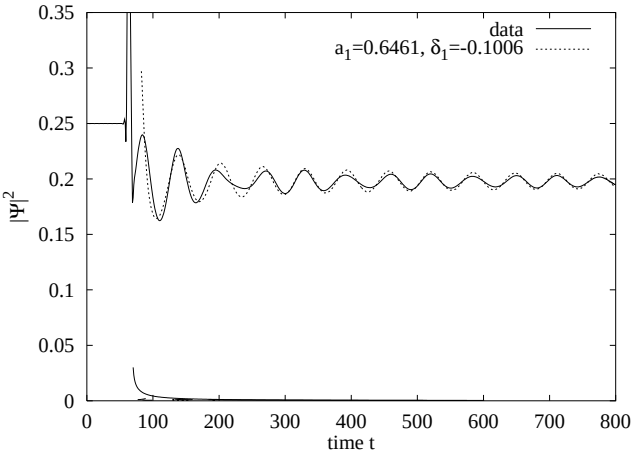

Fig. 14. $|\Psi|^2$ of the simulated amplified soliton with $a_1 = 0.6461 \pm 0.0400$, $\delta_1 = -0.1006 \pm 0.0100$ in comparison with the reflected soliton with the parameters $v_0 = 0.8, x_0 = 0, V_0 = 0.5$.

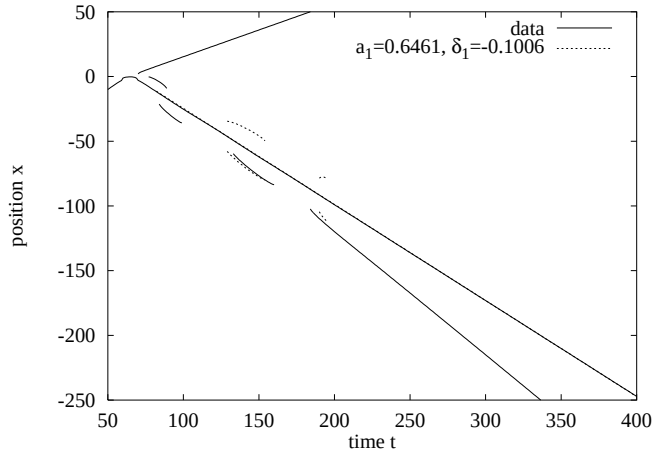

Fig. 15. Comparison between the position of the local maxima of the simulated solution and the reflected soliton as in Fig. 14.

those cases the reflected soliton has a larger amplitude than the nonsolitary wave emitted during the interaction. Thus, effects due to interferences are rather small. If their amplitudes are of the same order, they strongly interfere and deform the shape of the amplified soliton. A way to avoid that problem is to wait very long until the radiation either has passed through the soliton or is dispersed. But this would require very long simulations. Another problem is that in general the oscillation periods of the reflected soliton get very large which requires a very long simulation time, too.

Another comparison between data and theory is shown in Figs. 14 and 15 for the situation $v_0 = 0.8$, $V_0 = 0.5$, and $x_0 = 0$. The simulation and the amplified soliton show only small discrepancies, mainly during the first three

oscillation periods. The interference is also the reason why the side-maxima of the radiation emitted by the amplified soliton are not reproduced correctly. The rest is quantitatively very well reproduced.

In summary, each of the solitary waves after the scattering can be described as an amplified soliton, except for a very short time during the collision process. It is described by means of only two parameters: the reflected resp. transmitted mass and the height of the soliton in the limit $t \to \infty$. Since these states are not solitons at finite times, they emit radiation. This happens continuously and the amount radiated until a time t is proportional to $\sqrt{t^{-1}}$ [41]. Indeed, we see that the amplitude of the linear waves does not decay exponentially [42]. In the limit $t \to \infty$, the solitary waves converge to solitons with defined shapes. The total amount of radiation lost is simply

$$N_0 - N_\infty = 2\frac{\delta^2}{a}\,. \tag{33}$$

But this means that the overall amount of radiation produced during the whole scattering process is in general much bigger than one might have supposed at first sight. For steeper ramps more than 10% of the mass and even slightly more of the energy is eventually radiated by the two amplified solitons leaving the ramp into two directions. Summing up all effects we find that in cases where the potential is of the same order as the soliton's kinetic energy and the slope is steep, about one fourth of the initial mass and energy is radiated. Otherwise the loss is smaller. The percentage of radiation decreases systematically with decreasing slope. In the limit of very flat ramps ($x_0 \to \infty$) it tends to 0.

4.2 Oscillation period of the solitons amplitude

Kath and Smyth [34] derived two formulas which estimates the period of the amplitude oscillations for an amplified soliton with shape (27). For this, they used an alternative method to describe the time evolution of the soliton, namely a Lagrangian approach [43]. This leads to four approximate differential equations. These coupled ODE's allow to predict the time evolution of the soliton's parameters including the "mass loss" due to dispersive radiation. Their results are in agreement with the full numerical solution of the NLSE.

As we have shown above, the assumption that the solitary wave after the scattering is described by an amplified soliton with suitable values for a and δ, seems to be valid in a wide range of external perturbations. Thus we can apply their formulas to our data to see how far they agree.

For small perturbations, it was shown in [34] that the period of the amplitude

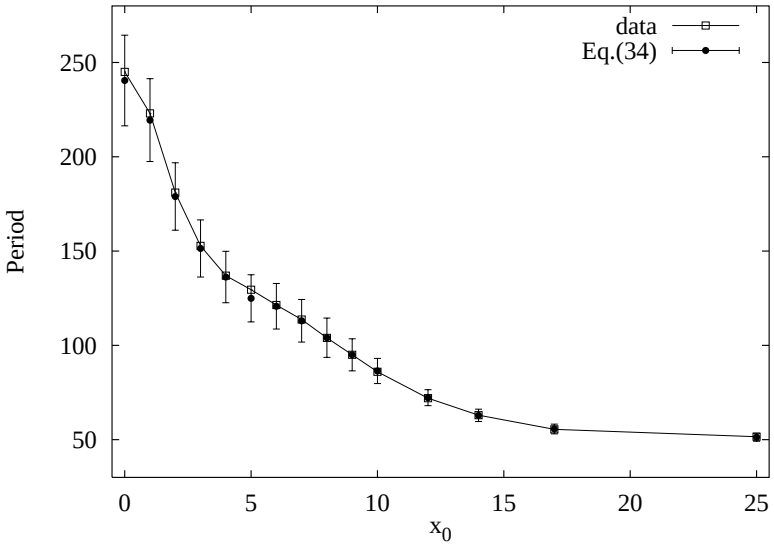

Fig. 16. Oscillation periods of the transmitted soliton (data), compared with the ones calculated using Eq.(34). Small values of x_0 correspond to large $|\delta|$ and large x_0 to small $|\delta|$. The initial parameters of the system are $V_0 = 0.30$, $v_0 = 0.8$ and $a_0 = 0.5$. The errors on the directly measured data are not shown, but are roughly half as big as those plotted for Eq.(34).

oscillations is the same as that of the phase oscillations of the pure soliton at time $t = \infty$:

$$T \simeq \frac{4\pi}{\kappa^2} \; . \tag{34}$$

For finite perturbations ($|\delta| > 0$), the same authors found (using our notation)

$$T = \frac{\pi^2}{\kappa^2} \left[1 - \left(1 - \frac{a^2}{(a+\delta)^2} \right)^2 \right]^{-\frac{3}{2}} \; . \tag{35}$$

Notice that this does not agree with Eq.(34) for $|\delta| \to 0$, as the authors of [34] already pointed out.

Measured oscillation periods are plotted in Figs. 16 and 17 against x_0 for two different velocities. These are comparisons with the predicted values of Eq.(34), where we have substituted $\kappa = a + 2\delta$. The values predicted by Eq.(35) do not fit the data in a sufficient manner. It predicts smaller values for $x_0 > 16$ ($v_0 = 0.8$) resp. $x_0 > 10$ ($v_0 = 0.6$) and much larger values for $x_0 \to 0$. But the simple Eq.(34) shows a surprisingly good agreement for all data points in both cases.

We could conclude from this that the disturbance of the soliton's amplitude

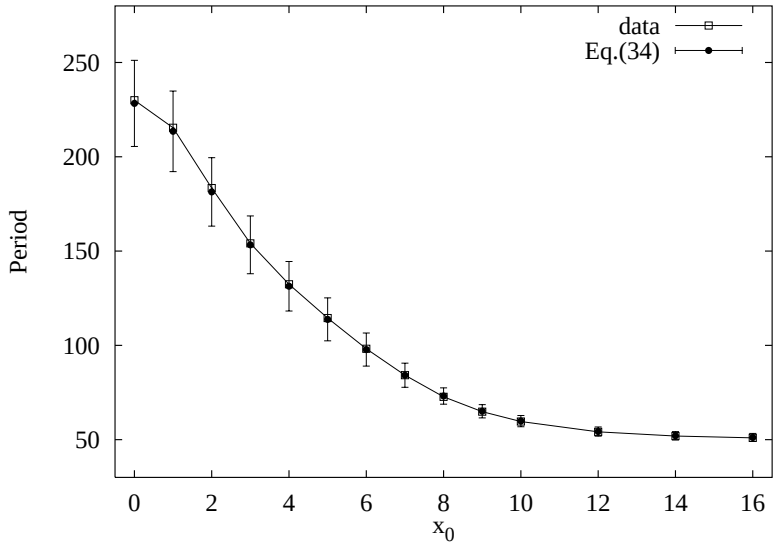

Fig. 17. The same as in Fig. 16 but for different initial parameters ($V_0 = 0.17$, $v_0 = 0.6$, $a_0 = 0.5$).

we are dealing with seems to be not as large as expected. Namely, in the sense that Eq.(34)—meant to be valid only for very small disturbances—predicts the correct time periods. This is astonishing, because we found an reduction of the soliton's amplitude up to 25%! This would mean that the valitiy range of Eq.(34) is much larger than assumed in [34].

5 Summary and conclusions

In this paper we found that solitons break up in general when hitting a potential threshold. If the slope is very steep and the potential height is either very low or very high compared to the soliton's kinetic energy ($K_0 \gg V_0$ or $K_0 \ll V_0$), the soliton acts like a Newtonian particle. The same behavior is seen if the slope is rather flat ($V_0/x_0 \ll 1$) for most values of V_0. This includes the fact that in those cases only very little energy and mass is transfered into radiation. In such cases only one soliton with nearly constant height exists during the whole simulation time. The amplitude of this solitons shows small oscillations with a period, that is the period of the phase oscillation of the undisturbed soliton.

The complexity of the outgoing state depends on the parameters of the potential and of the soliton, but most frequently the soliton breaks into two solitons of different mass. We have shown that these solitons can be described by amplified solitons whose parameters a and δ can be evaluated from the data. Additionally, the period of the amplitude oscillation can easily be calcu-

lated. The scattered solitons are accompanied by radiation, which is emitted continuously and whose amplitude decays proportional to $1/\sqrt{t}$ in time for large times. The fact that the radiation decays only with a power law raises some problems with the transmission of information via optical fibers [42].

In some region of the (x_0, V_0)-plane the soliton is almost fully reflected even if its kinetic energy is slightly larger than the potential. This is due to the emission of radiation. The energy of the soliton is reduced thereby, whence it cannot overcome the ramp and is reflected. The associated jumps in the transmission coefficients are rather sharp and the slope where this happens depends on the hight of the potential. The window in slopes where the soliton is reflected shrinks if the height of the potential is lowered. At a critical value $V_{0,c}$ this feature disappears and the transmission coefficients rise monotonically. As the potential height tends to the value of the soliton's kinetic energy, the right border of the window tends to $+\infty$.

In this paper we have mostly studied the NLSE with an external potential that has the form of a linear ramp with variable hight and slope. We have applied an optimized fourth-order symplectic integrator in our simulations. The integrator is optimized in the sense that it takes into account the symplectic structure of the NLSE and the fact that the kinetic energy is bilinear in Ψ_x. It has a very good long-time stability.

It is very easy to apply this algorithm to NLSEs with other external potentials, such as one or more impurities, a series of step functions or any smooth function. In the same way other Hamiltonian disturbances can be treated, e.g. terms like $|\Psi|^{2p}\Psi$. In order to study the collision of two solitons (a fast one and a slow one) or of three solitons (a fast one crossing two interacting slow ones) [44,45], an integrator with good long-time stability is needed. We believe that the integrator used in the present work can be very useful in further simulations of partial differential equations of such a type. This numerical method can also be easily and staightforward applied to the NLSE with a varying nonlinear term or to higher dimensional and coupled NLSEs. Thus the vector NLSE, which describes e.g. the propagation of light in a birefringent optical fiber, can be simulated with such an algorithm. Also soliton switching and splitting can be simulated by using this algorithm.

Acknowledgements

The author would like to thanks Prof. P. Grassberger, Dr. Yu.S. Kivshar and B.A. Malomed for fruitful discussions.

This work was supported by DFG within the Graduiertenkolleg "Feldtheore-

tische und numerische Methoden in der Elementarteilchen- und Statistischen Physik", and within SFB 237.

Appendix

A Symplectic integration

Here we briefly describe the integration method which we have used to simulate the NLSE.

As we have already mentioned, the NLSE is a Hamiltonian system. Thus, it is natural to apply to it integration routines which were developed during the recent years and whose main characteristic is that they preserve the Hamiltonian structure [46–48]. The latter is not true e.g. for standard methods as e.g. Runge-Kutta or predictor-corrector. Such 'symplectic' integrators (the simplest of which is the well known Verlet or 'leap frog' algorithm) have been applied already to the linear [49–52] and nonlinear [32,53–56] Schrödinger equations.

The most popular algorithms of this type are split-operator methods. They depend on the Hamiltonian being a sum of two terms A and B, each of which can be integrated explicitly. Then one uses the Baker-Campbell-Hausdorff theorem to approximate $e^{i(A+B)t}$ by a product of factors $e^{i\alpha_k At}$ and $e^{i\beta_k Bt}$, where α_k and β_k are real numbers satisfying among others $\sum_k \alpha_k = \sum_k \beta_k = 1$. The error is given by higher order commutators of A and B. In particular, we apply a fourth-order method introduced by McLachlan and Atela [57] which is applicable if one of the third order commutators vanished identically. We found that this method should be applicable to our problem, and that it is indeed numerically very precise, indicating that the McLachlan-Atela method is the method of choice for a wide class of problems.

The NLSE is a classical Hamiltonian system with Poisson bracket

$$\{\Psi^*(x), \Psi(y)\} = i\delta(x-y) \tag{A.1}$$

and Hamiltonian $H = E$. This implies in particular that it can be written as

$$\dot{\Psi} = \{\Psi, H\} = \mathcal{H}\Psi\,, \tag{A.2}$$

where the linear ('Liouville') operator $\mathcal{H}$ is defined as $\mathcal{H}\cdot = \{\cdot\,, H\}$. Split-operator methods can be applied by splitting $\mathcal{H} = \mathcal{T} + \mathcal{V}$, where $\mathcal{T}$ and $\mathcal{V}$ are

the Liouvilleans corresponding to $\frac{1}{2}\int \mathrm{d}x|\partial_x\Psi|^2$ and $\int \mathrm{d}x(-\frac{1}{2}|\Psi|^4 + V|\Psi|^2)$,

$$\mathcal{T}\Psi = \frac{i}{2}\partial_x^2\Psi \ , \quad \mathcal{V}\Psi = i(|\Psi|^2\Psi - V\Psi) \ . \tag{A.3}$$

In [57], a fourth-order algorithm was introduced which minimizes the neglected fifth order terms in the Baker-Campbell-Hausdorff formula for Hamiltonians for which

$$[[[\mathcal{T},\mathcal{V}],\mathcal{V}],\mathcal{V}] \equiv 0 \ . \tag{A.4}$$

This applies obviously to Hamiltonians with $T = \frac{1}{2}(p, M^{-1}p)$, $V = V(x)$, with M a constant mass matrix and $\{q_i, p_k\} = \delta_{ik}$, since in the Baker-Campbell-Hausdorff formula each commutator with V acts as a derivative operator on any function of p. In [51] it was shown that this algorithm can also be applied to the linear Schrödinger equation where it gives better performance than the general fourth-order algorithm [46] which does not take into account this special structure. In [32] it was shown that eq. (A.4) holds also for $\mathcal{T}$ and $\mathcal{V}$ defined in eq. (A.3) and the McLachlan-Atela method can thus also be used for the NLSE.

The coefficients α_k and β_k for the McLachlan-Atela method are listed in [57,51]. Our implementation involves a spatial grid with Fourier transformation after each half step [51]. [2]

Since $\mathcal{T}$ and $\mathcal{V}$ both conserve the mass exactly, N should be conserved up to round-off errors. This was checked numerically, relative errors typically were of order 10^{-11}. Energy is not conserved exactly, and its error was $\approx 10^{-7}$ after an evolution time $t = 500$ with an integration step $\Delta t = 0.0025$. The precise value of the error depends of course on the parameters of the soliton and on x_0. We checked carefully that our final results were independent of the time step and of the spatial discretization Δx. It was checked that the algorithm is indeed fourth-order, and is more precise than the general fourth-order symplectic [46] and the leap-frog (second-order symplectic) algorithms.

The derivatives of Ψ and Ψ^*, which have to be calculated numerically, were computed in Fourier space, as this is much more precise than taking finite differences in x-space. Using the latter, the relative error of the energy conservation would have been of the order 10^{-4} instead of 10^{-7}.

[2] As an alternative to the Fourier transform one can perform these steps also in x-space [58]. Instead of a FFT, one has to perform a convolution with the Greens-function of $\mathcal{T}$ in each time step. Practically, both methods are roughly equally fast.

References

[1] J.S. Russell, *Report of the committee on waves*, Report of the 7th Meet. Brit. Assoc. Adv. Sci., Liverpool 1838.

[2] J.S. Russell, *Report on waves*, Report of the 14th Meet. Brit. Assoc. Adv. Sci., London 1844.

[3] D.J. Korteweg and G. de Vries, *Phil. Mag. Ser. 5* **39** (1895) 422.

[4] C.S. Gardener *et al.*, *Phys. Rev. Lett.* **19** (1967) 1095.

[5] C.S. Gardener *et al.*, *Comm. Pure Appl. Math.* **27** (1974) 97.

[6] V.E. Zakharov and A.B. Shabat, *Sov. Phys.-JETP* **111** (1972) 62.

[7] M.J. Ablowitz *et al.*, *Phys. Rev. Lett.* **31** (1973) 125.

[8] M.J. Ablowitz *et al.*, *Stud. Appl. Math.* **53** (1974) 249.

[9] H. Hasimoto and H. Ono, *J. Phys. Soc. Jpn.* **52** (1983) 4129.

[10] A.P. Fordy, *Soliton theory: A survey of results*, Manchester University Press, Manchester 1990.

[11] G.L. Lamb, Jr., *Elements of Soliton Theory*, Wiley Toronto 1980.

[12] J.P. Gordon, *J. Opt. Soc. Am.* **B 9** (1992) 91.

[13] M. Chbat *et al.*, *J. Opt. Soc. Am.* **B 10** (1993) 1386.

[14] D. Anderson *et al.*, *J. Opt. Soc. Am.* **B 11** (1994) 2380.

[15] Yu.S. Kivshar *et al.*, *Phys. Rev.* **A 41** (1990) 1677.

[16] Yu.S. Kivshar and M.L. Quiroga-Teixeiro, *Phys. Rev.* **A 48** (1993) 4750.

[17] A. Hasegawa and F. Tapert, *Appl. Phys. Lett.* **23** (1973) 142.

[18] L.E. Mollenauer, R.H. Stolen, and J.P. Gordon, *Phys. Rev. Lett.* **45** (1980) 1095.

[19] J. Fricke, *Physik in unserer Zeit* **23** (1992) 256.

[20] F.X. Kärtner, *Physik in unserer Zeit* **26** (1995) 152.

[21] R. Jackiw, *Rev. Mod. Phys.* **49** (1977) 681.

[22] V.I. Karpman, *Phys. Scr.* **20** (1979) 462.

[23] A. Bondeson *et al.*, *Phys. Scr.* **20** (1979) 479.

[24] Yu.S. Kivshar, A.M. Kosevich, and O.A. Chubykalo, *Sov. Phys. JETP* **66** (1987) 545.

[25] Yu.S. Kivshar and B.A. Malomed, *Rev. Mod. Phys.* **61** (1989) 763.

[26] Y. Nogami and F.M. Toyama, *Phys. Rev.* **E 49** (1994) 4497.

[27] R. Knapp, *Physica* **D 85** (1995) 496.

[28] M.A. Moura, *J. Phys.* **A***: Math. Gen.* **27** (1994) 7157.

[29] Y. Nogami and F.M. Toyama, *Phys. Lett.* **A 184** (1994) 245.

[30] F.M. Giusto *et al.*, *Physica* **D 11** (1984) 227.

[31] T.A. Minelli and A. Pascolini, *Il Nuovo Clim.* **B 85** (1985) 1.

[32] H. Frauenkron and P. Grassberger, *J. Phys.* **A***: Math. and Gen.* **28** (1995) 4987.

[33] Hsing-Hen Chen and Chuan-Sheng Liu, *Phys. Rev. Lett.* **37** (1976) 693.

[34] W.L. Kath and N.F. Smyth, *Phys. Rev.* **E 51** (1995) 1484.

[35] P.G. Drazin and R.S. Johnson, *Solitons: An introduction*, Cambridge University Press 1989.

[36] D.J. Kaup and A.C. Newell, *Proc. R. London Soc.* **A 361** (1978) 413.

[37] Yu.S. Kivshar, A.M. Kosevich, and O.A. Chubykalo, *Phys. Lett.* **A 125** (1987) 35.

[38] H. Frauenkron and P. Grassberger, *Phys. Rev.* **E 53** (1996) 2823.

[39] Yu.S. Kivshar, Z. Fei, and L. Vázquez, *Phys. Rev. Lett.* **67** (1991) 1177.

[40] Z. Fei, Yu.S. Kivshar, and L. Vázquez, *Phys. Rev.* **A 46** (1992) 5214.

[41] J. Satsuma and N. Yajima, *Prog. Theor. Phys. Suppl.* **55** (1974) 284.

[42] E.A. Kuznetsov *et al.*, *Physica* **D 87** (1995) 201.

[43] D. Anderson, *Phys. Rev.* **A 27** (1983) 3135.

[44] Yu.S. Kivshar and B.A. Malomed, *Phys. Lett.* **A 115** (1986) 377.

[45] H. Frauenkron, Yu.S. Kivshar and B.A. Malomed, *Phys. Rev.* **E 54** (1996) R2244.

[46] H. Yoshida, *Phys. Lett.* **A 150** (1990) 262.

[47] H. Yoshida, *Cel. Mech. Dyn. Astron.* **56** (1993) 27.

[48] J.M. Sanz-Serna, *Physica* **D 60** (1992) 293.

[49] A.D. Bandrauk and Hai Shen, *Chem. Phys. Lett.* **176** (1991) 428.

[50] K. Takahashi and A. Shudo, *Dynamical fluctuations of observables and the ensemble of classical trajectories*, submitted to J. Chem. Phys. 1992.

[51] H. Frauenkron and P. Grassberger, *Int. J. Mod. Phys.* **C 5** (1994) 37.

[52] A. Rouhi and J. Wright, *Comput. Phys. Commun.* **85** (1995) 18.

[53] J.A.C. Weideman and B.M. Herbst, *SIAM J. Numer. Anal.* **23** (1986) 485.

[54] D. Pathria and J.L. Morris, *J. Comput. Phys.* **87** (1990) 108.

[55] A.D. Bandrauk and Hai Shen, *J. Phys.* **A***: Math. Gen.* **27** (1994) 7147.

[56] R.I. McLachlan, *Numer. Math.* **66** (1994) 465.

[57] R.I. McLachlan and P. Atela, *Nonlinearity* **5** (1992) 541.

[58] A. Torcini, H. Frauenkron, and P. Grassberger, *Physica* **D 103** (1997) 605.